Materials Chemistry and Physics 290 (2022) 126510

Contents lists available at ScienceDirect

Materials Chemistry and Physics

journal homepage: www.elsevier.com/locate/matchemphys

# Fabrication of $In_2Te_3$ nanowalls garnished with ZnO nanoparticles and their field emission behavior

Muhammad Safdar[a,*], Muhammad Waqas[a], Nimra Jabeen[a], Ahmad Saeed[a], Faheem K. Butt[c], Shahzad Murtaza[a], Misbah Mirza[b,**]

[a] *Institute of Chemistry, Khwaja Fareed UEIT, Rahim Yar Khan, Pakistan*
[b] *Department of Physics, The Women University Multan, Pakistan*
[c] *Department of Physics, University of Education, Lahore, Pakistan*

## HIGHLIGHTS

- First time vertical growth $In_2Te_3$ nanowalls, single crystalline, 50 nm thin.
- Two-dimensional (2D) vertical oriented indium sesquitelluride ($In_2Te_3$) nanowalls, and ZnO/$In_2Te_3$ nano heterostructures.
- Field emission analysis of $In_2Te_3$ nanowalls.
- Field emission improvement by ZnO nanoparticles garnished on $In_2Te_3$ nanowalls.
- Turn on field 2.1 $V\mu m^{-1}$.

## GRAPHICAL ABSTRACT

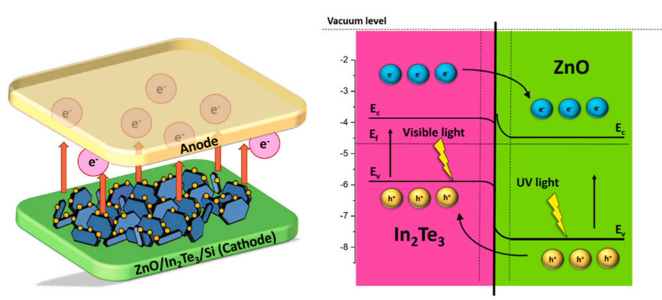


## ARTICLE INFO

*Keywords:*
Indium sesquitelluride 2D nanowalls
ZnO nanoparticles
Field emission
Turn on field
Current degradation
and ZnO/$In_2Te_3$ nanoheterostructures

## ABSTRACT

Two-dimensional (2D) vertical oriented indium sesquitelluride ($In_2Te_3$) nanowalls, and ZnO/$In_2Te_3$ nano-heterostructures were grown on Si substrate via simple chemical vapor deposition (CVD) technique. The monitored $In_2Te_3$ nanowalls are single crystalline, 120–150 nm in size and approximately 50 nm thin. Indium sesquitelluride ($In_2Te_3$) has a suitable band gap for optoelectronic and energy field applications but its field emission properties have not been investigated yet. For the first time, $In_2Te_3$ structures have been subjected for field emission analysis which pointed out reasonable properties of field emission. Owing to field emission improvement, ZnO nanoparticles were garnished on $In_2Te_3$ nanowalls. This causes an impressive reduction in turn on field which approaches to 2.1 $V\mu m^{-1}$ as compared to pure $In_2Te_3$ nanowalls 3.2 $V\mu m^{-1}$. In addition, excellent emission stability without significant current degradation is noted. These findings indicated that 2D nanowalls of $In_2Te_3$ and ZnO/$In_2Te_3$ nanoheterostructures have great potentials for future applications in the energy field.

* Corresponding author.
** Corresponding author.
*E-mail address:* msafdarsami@yahoo.com (M. Safdar).

https://doi.org/10.1016/j.matchemphys.2022.126510
Received 13 April 2022; Received in revised form 11 July 2022; Accepted 11 July 2022
Available online 30 July 2022
0254-0584/

## 1. Introduction

In research, various field emission investigations of zero-dimensional (quantum dot), one-dimensional (quantum wire) and two-dimensional (quantum film) semiconductor nanostructures of carbon, GeAs, ZnO, $In_2O_3$, $SnO_2$, $TiO_2$, CdSSe and SiC frameworks exhibited optimal optoelectronics properties because of high surface area to volume ratio, high density, small radius of curvature, and special morphology [1–6]. Lately, 2D nanostructures like nanosheets, nanowalls and their heterostructures have attained intense focus of scientific society because of their unique physical properties, extraordinary geometry and high aspect ratio for nanoscale devices in nanoelectronics and nanophotonics [7]. Because of the consistent and high crystal quality of 2D nanostructures, charge carriers can flow via interatomic sites without scattering. These leads upgraded electrical conductivity and unrivaled field emission characteristics [8]. In specific, the field emission properties of 2D nanostructures have appealed attention because of their greater field emission phenomena. Field emission related with quantum tunneling phenomenology has attained in broad consideration in vacuum electron gadget such as high energy accelerators, panel displays, microwave amplifiers and X-ray generators applications, due to its transient reaction and low power cost characteristics [9]. Field emission depicts the discharge of electrons from a conducting substrate into vacuum by means of electron tunneling via the potential barrier surface [10,11]. As tunneling is a delicate test of the electronic spectrum, field emission has regularly been applied as a valuable spectroscopic instrument for characterization of bulk material [12]. Experiments exploiting nanostructured emitters disclosed deviations from regular theory connoting that tunneling takes place in these frameworks through discrete energy levels, shaped in the nano-edges because of spatial constrains [13]. In this regard, nanowalls arrays of GaS, $TiO_2$, and ZnO have been studied [14–17]. Moreover, the doping, core shell, hierarchical and heterostructure fabrications of nanostructures are important aspects to explore field emission as well as other electrical and optical properties of semiconductors [18]. With interest as to potential and competitive heterostructures analysis of ZnO/ZnS, ZnO/CdS and ZnO/$Ag_2S$ displayed significant lower turn on field compared to pure ZnO [19–22].

Indium telluride is a vital III−VI semiconductor compound with direct band gap of about 1.19eV which depicts an efficient material with enhanced photoelectric properties. However, past research on $In_2Te_3$ is up to great extent considering thin film for gas sensors, thermoelectric power generators and memory devices. Contrasted thin film materials, the one of exceptional physical and chemical properties of nanostructured semiconductors make them perfect in developing as well outlining highly useful nanodevices like nanowires photo detectors contributed by our group [23–25].

In this article, by streamlining the deposition parameters in the CVD, we effectively express the preparation of high quality, single crystalline $In_2Te_3$ nanowalls. For the first time, we synthesized and characterized 2D vertical nanowalls of $In_2Te_3$, along with fabricated $In_2Te_3$/ZnO nanoheterostructures. Encouragingly, $In_2Te_3$ nanowalls and $In_2Te_3$/ZnO nanoheterostructures devices were fundamentally inspected for field emission properties systematically. The device reveals much better performance turnout voltage. We considered these outcomes as the CVD developed $In_2Te_3$ nanowalls, and $In_2Te_3$/ZnO nanoheterostructures may be potential candidate for field emission devices and are promising possibility for telluride-based chalcogenides applications in high affectability for the novel optoelectronic appliances.

## 2. Experimental

### 2.1. Synthesis of indium telluride ($In_2Te_3$)

$In_2Te_3$ nanowalls were synthesized on Si substrates using horizontal vacuum tube furnace along the one temperature zone. The growth substrates were cleaned by a standard cleaning process prior to load in furnace tube. $In_2Te_3$ nanowalls source material, $In_2Te_3$ powder was filled in middle of the quartz tube and Si substrates deposited at distance 15–20 cm in downstream area. Firstly, quartz tube stimulated as evacuated, sealed, and flushed several times with great purity Ar and $H_2$ gas to provide oxygen free environment. During this process, Ar gas sustained with a constant flow rate by keeping 150 Torr tube pressure. Temperature of the furnace was modified to 600–700 °C for source and 300–400 °C for substrate. Overall reaction process was managed for 60 min. Then furnace was allowed to cool down naturally for attaining room temperature.

### 2.2. Garnishing of ZnO particles on $In_2Te_3$ nanowalls

The ZnO nanoparticles deposition on $In_2Te_3$ nanowalls were also performed in same single temperature zone at temperature 600 °C with temperature rising rate of 30 °C/min in a horizontal vacuum tube furnace. The evaporation source ZnO (99.99%, alfa aesar) was placed on a boat, positioned in the center and $In_2Te_3$ nanowalls substrate at 400 °C, 8–10 cm downstream of tube furnace. The source evaporation and deposition time was 10 min.

### 2.3. Characterizations

The morphologies of $In_2Te_3$ grown structures were characterized by field emission scanning electron microscopy (FESEM) S4800 (Tokyo, Japan) at 10 KV. Selected area electron diffraction (SAED), Transmission electron microscopy (TEM), and the high-resolution transmission electron microscope (HRTEM) were performed at an accelerating voltage of about 200 kV on FEI Tecnai F20. The SEM attached; energy dispersive X-ray spectroscopy (EDX) was used to identify composition of crystal structure.

### 2.4. Measurement of field emission

Field emission measurements were operated at the room temperature under two parallel plates arranged in a vacuum chamber. Base pressure for the chamber was executed by using vacuum pump at $10^{-7}$Pa and Keithley picoammeter of semiconductor characterization system was used to measure emission current of devices. It is included that nanostructured Si substrates hold $1 \times 1$ $cm^2$ area for emission, produces 1 $\mu Acm^{-2}$ current density by applied field (turn on field) [26, 27].

## 3. Results and discussion

FESEM images presenting morphologies of the as fabricated $In_2Te_3$ and $In_2Te_3$/ZnO nanostructures in Fig. 1. The dense and uniform growth of $In_2Te_3$ and $In_2Te_3$/ZnO are displayed in FESEM images. The result in Fig. 1(a) and (c) reveals that $In_2Te_3$ nanostructures grown in the standing, perpendicular to substrate, vertical 2D nanowall forms. The high magnification FESEM image of nanowalls in Fig. 1(c) depicting that these nanowalls are interconnected with each other forming a net shaped film, and thickness of nanowalls is in the range of 50 nm. It is apparent in FESEM images (b) and (d) that pristine $In_2Te_3$ nanowalls are garnished with nanoparticles of ZnO, demonstrating hierarchical $In_2Te_3$/ZnO nanoheterostructures. The high magnification FESEM image of $In_2Te_3$/ZnO nanoheterostructures in Fig. 1(d), showing that ZnO particles are covering top edges of nanowalls with high density and diameter of ZnO nanoparticles is in the range of 50 nm. It is observed, while assembling ZnO nanoparticles, morphology of nanowalls did not change. The $In_2Te_3$/ZnO nanostructures were evaluated through XRD (Fig. S†1) and Raman analysis (Fig. S†2) which provided phase information and purity of these nanostructures. The segments c and d of Fig. 1 are energy dispersive X-ray (EDX) pattern of pristine $In_2Te_3$ nanowalls and $In_2Te_3$/ZnO nanoheterostructures, respectively. The EDX spectrum of pristine $In_2Te_3$ nanowalls signaled its pure composition of In and Te

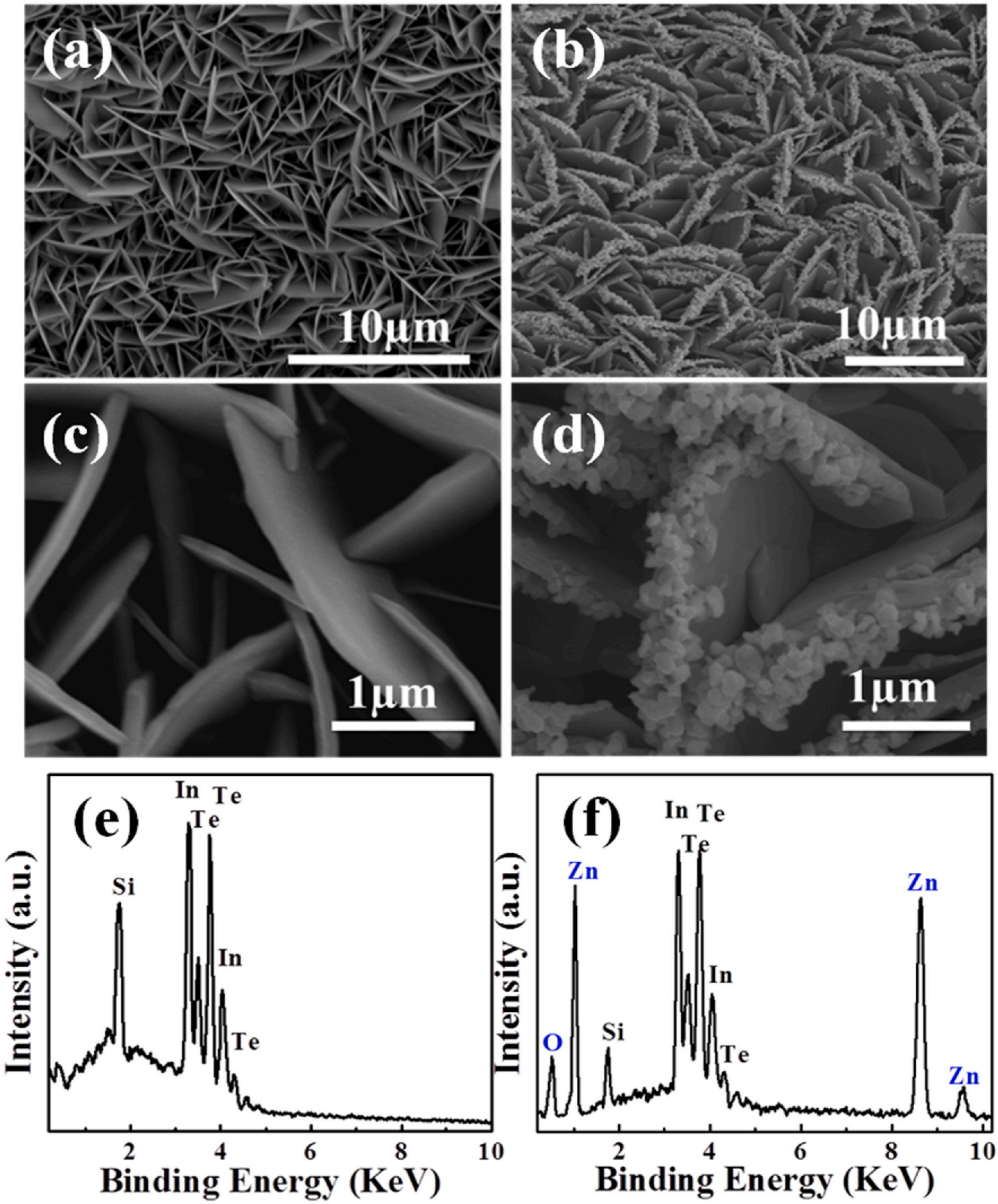


**Fig. 1.** (a & c) FESEM images of $In_2Te_3$ nanowalls (b & d) FESEM images $In_2Te_3$/ZnO nanoheterostructures. (e & f) Energy Dispersive X-ray (EDX) pattern of pristine $In_2Te_3$ nanowalls and $In_2Te_3$/ZnO nanoheterostructures, respectively.

with 2:3 atomic ratio. In addition, new peaks emerge when EDX pattern of $In_2Te_3$/ZnO nanoheterostructures collected, which are attributed to ZnO, and it was exactly as expected after nanoparticles garnished using ZnO source in furnace. Moreover, no additional peaks are noticed which mean absence of impurities in either of the samples.

For step up, investigation about morphology and crystal structure of pristine $In_2Te_3$ nanowalls and ZnO garnished $In_2Te_3$ nanoheterostructures, information was collected via TEM and HRTEM measurements as results shown in Fig. 2. The TEM images of $In_2Te_3$ nanowalls presented in Fig. 2(a), indicating that nanowalls are 2D nanostructure with smooth periodic pattern, hence single crystalline structure as shown in Fig. 2(b). The edge surface is cleaned and uniformed on atomic scale, as well there are no amorphous layers have been detected on its surface.

Accordingly, the lattice fringes image representing lattice spacing 3.5 Å, which correspond to the (511) plane of $In_2Te_3$ [28]. The appearance of bcc $In_2Te_3$ crystal lattice fringes, (511) plane is also confirming the formation of $In_2Te_3$ as it is high intensity peak appeared in XRD pattern reported in our previous work [29]. Fig. 2(c), TEM images show more detailed information about $In_2Te_3$/ZnO nanoheterostructures, i.e., ZnO nanoparticles are polygonal shape, 100 nm in size and well adhered to $In_2Te_3$ nanowalls. The HRTEM taken from an

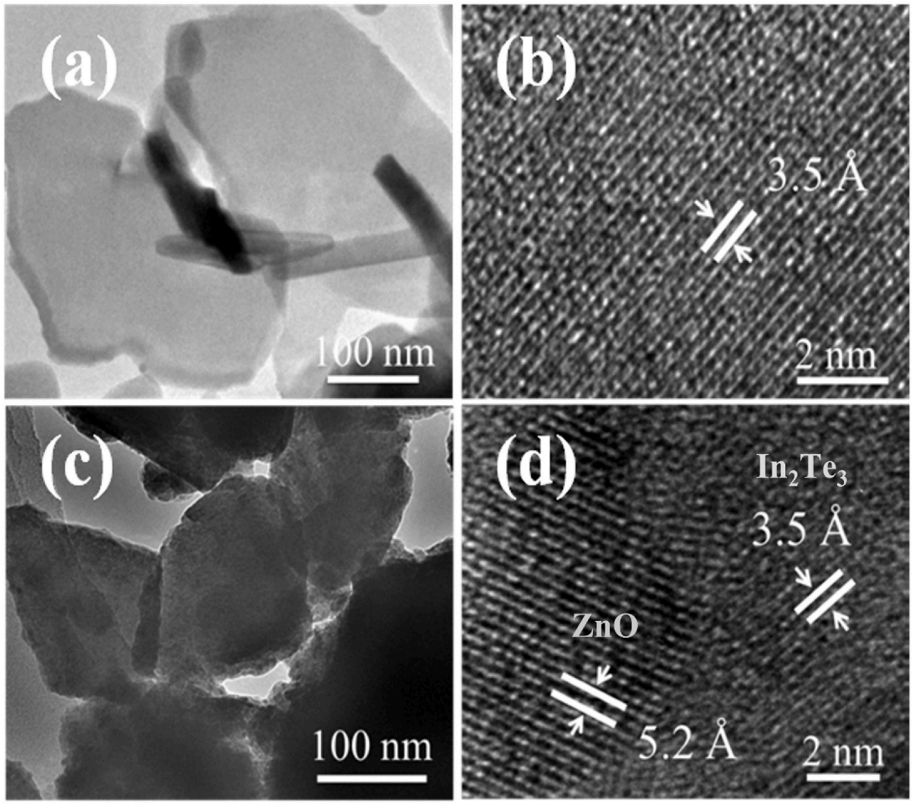


**Fig. 2.** (a) TEM image of 2D $In_2Te_3$ nanoplates, (b) HRTEM image of $In_2Te_3$ nanoplates, (c) TEM image of $In_2Te_3$/ZnO nanoheterostructures and (d) HRTEM image from interface area of $In_2Te_3$/ZnO heterojunctions.

interface position confirm the excellent heterojunctions of $In_2Te_3$/ZnO nanoheterostructures as shown in Fig. 2(d). The lattice spacing 3.5 Å and 5.2 Å correspond to (511) plane and (002) plane, which speak for the presence of $In_2Te_3$ and ZnO respectively [29,30]. These results reveal that $In_2Te_3$ structure stays intact even after the ZnO nanoparticles attachment. The growth of nanowalls happened due to vapor solid (VS) process growth mechanism as we have not used any catalyst as well as droplet on the surface not observed in microscopic images. The presence of In and Te in stochiometric ratio evidence for right In–Te flux ratio at the growing substrate and proper growth temperature at substrate area where perfect crystal aggregation led to formation of nanowalls. HRTEM analysis indicating the growth happened along the [511] crystalline orientation of the $In_2Te_3$ crystal. For the second stage of heterostructures growth, ZnO powder was evaporated in same horizontal tube furnace which condensed on $In_2Te_3$ nanowalls assisted Si substrate. The epitaxially condensed and absorbed vapors of ZnO nucleate onto $In_2Te_3$ nanowalls and grow to form polygonal structure. The $In_2Te_3$ nanowalls top surface kinetically favors the growth of polygonal structure. The formation of ZnO confirmed by EDX as well as HRTEM information of polygonal structures.

### 3.1. Field emission properties

Field emission is an electron escape process from the solid surface in the presence of a significantly higher electric field because of tunneling effect. Morphology, size (radius of edge and tip), optimum density, work function, band gap are very fundamental factors for the FE intensity. A cathode surface should have high surface to volume ratio, sharp edges as electrons emit from them could easily transfer to anode in presence of an applied electric field [31]. Two-dimensional semiconductor nanostructure arrays i.e., nanowalls often own typical field emission properties which can be improved by heterostructures or heterojunctions structures. In this context, we fabricated $In_2Te_3$ nanowalls and $In_2Te_3$/ZnO heterostructures semiconducting material for the first time. Synthesized $In_2Te_3$ nanowalls array and $In_2Te_3$/ZnO heterostructures are homogenized with regular pattern and have nanoscale edges.

The field emission current characteristics are analyzed as emission current density (J) plotted versus applied electric field (E), depicted in Fig. 3. The (J-E) plot revealing that the current density exponentially rises along electric field. The current density (J) is valuated as $J = I/A$, where, I is the emission current and A is the total area of the emitter, and electric field E is represented $E = V/d$, where V is the applied voltage, and d is the distance between anode and cathode which are 5.01V and 0.2 mm (200 μm) respectively [26,32]. The turn-on field is 3.2 $V\mu m^{-1}$ of the pristine $In_2Te_3$ nanowalls and the $In_2Te_3$/ZnO nanoheterostructures having 2.1 $V\mu m^{-1}$ turn-on field. The $In_2Te_3$ nanowalls have a smaller work function and the greater aspect ratio, thus it is acceptable that electrons could be transmitted more conveniently through their thin edges. Field emission properties of the $In_2Te_3$/ZnO nanoheterostructures have been appreciably enhanced as compared to the $In_2Te_3$ nanowalls.

For $In_2Te_3$/ZnO nanoheterostructures junction, the notably improved F.E properties are credible because of two reasons, the increased emission sites on $In_2Te_3$/ZnO nanoheterostructures surface and decrease in the potential energy (P.E) barrier due to band bending and inevitable interfacial defects at the junction within $In_2Te_3$ and ZnO. Because of the small sizes, the garnished ZnO nanoparticles on the $In_2Te_3$ nanowalls function as additional emission sites and cause the increase in number of emission dots.

Moreover, the band energy diagram for $In_2Te_3$/ZnO nanoheterostructures junction along an applied electric field has been shown in Fig. 4. The band bending is useful for transfer of electrons from $In_2Te_3$ to ZnO and holes from the ZnO to $In_2Te_3$, which successfully decreases the recombining of hole-electron pairs. The defects and vacancies at interface can persuade defect energy bands ($E_{defects}$) within original energy bands. Electrons in $In_2Te_3$ conduction band could freely jump into the $E_{defects}$ and then transfer to the ZnO nanomaterials. Thus, the

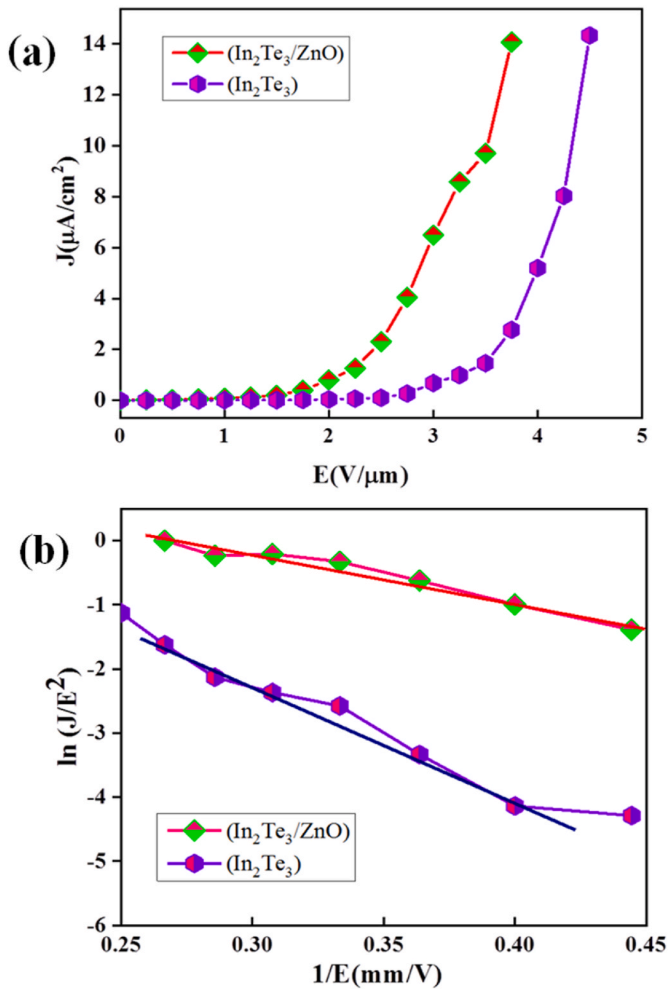


**Fig. 3.** (a) The field emission current as emission current density (J) plotted versus applied electric field (E). Part (b) shows the corresponding Fowler–Nordheim plot.

substantial numbers of electrons assemble on ZnO nanoparticles surface and are more easily ejected into the vacuum over successive Fowler-Nordheim tunneling below the high electric field. The free electrons also proceed towards anode.

Fowler-Nordheim plots, according to the results are shown in Fig. 4. This is exciting that F–N plots as for pristine $In_2Te_3$ and ZnO garnished $In_2Te_3$ nanowalls are straight lines, which depicts that emitting electron are mostly resulting from barrier tunneling electrons extracted through electric field. Field emission property by F–N (Fowler-Nordheim) equation, can be expressed as,

$$\ln (J/E^2) = (1/E)\ (-B\ \varphi^{3/2} / \beta) + \ln (A\beta^2 / \varphi) \quad (1)$$

Here, J is emission current intensity, E is applied electric field, β is field enhancement factor, A and B are the constants with values of 1.56 $\times 10^{-10}$ A $V^{-2}$ eV and 6.83 $\times 10^3$ $eV^{-3/2}$ V $mm^{-1}$, β is field enhancement factor, and φ is work function of transmitter material. In keeping with eq. (1), the slope of F–N plots possess an inverse ratio to the field enhancement factor β and could be accounted as follows [27]:

$$k_{slope} = -B\ \varphi^{3/2} / \beta \quad (2)$$

The field enhancement factor (β) of $In_2Te_3$ nanowalls and $In_2Te_3$/ZnO heterostructures has projected to be about 1805 and 3623, respectively. Earlier studies reveal that ZnO in bulk form possesses higher work function which may lower in its low scale dimensions (i.e. 5.3 eV) [33,34]. The $In_2Te_3$ nanostructures have comparable work function with ZnO (i.e., 4.97 eV) which is responsible for the suitable junction between the two phases. Therefore, the $In_2Te_3$/ZnO nanoheterostructures have improved field emission properties which can be explained due to enhanced electron emissions from the sharp edges of indium telluride facilitated by ZnO. This can be further described by tunneling ability of the electrons through nanoheterojunction of $In_2Te_3$/ZnO and high value for field enhancement factor of emitters. Metal-semiconductor junction at the interface of both nanostructures is formed which is due to difference in their work functions. When exciton occurs the electrons from $In_2Te_3$ flow towards the interface and assemble at surface of the ZnO to attain thermal equilibrium. The junction at the interface provides a small resistance contact between $In_2Te_3$ nanowalls and the ZnO nanostructures. This results in the fast transfer of ejected electrons from the fermi level of $In_2Te_3$ to ZnO edges under an external electric field [31]. The electrons saturated at ZnO tips are channeled into the vacuum for field emission properties through the subsequent Fowler-Nordheim tunneling by applied field. Furthermore, the field emission stability of $In_2Te_3$/ZnO nanostructures was tested at constant applied current of 3 V/$\mu m^2$ which showed no significant current loss Fig. S†3.

## 4. Conclusions

The field emission properties of all samples have been calculated and observed. It is apparent that $In_2Te_3$/ZnO nanoheterostructures have significantly enhanced field emission properties. $In_2Te_3$/ZnO heterostructures have better F.E phenomenon with lower turn-on field as compared to the pristine $In_2Te_3$ nanowalls. This is due to the chemical stability and reduced size of ZnO as well as high electrical conductivity and great mechanical strength of the $In_2Te_3$. The improved field enhancement factor (β) $In_2Te_3$/ZnO heterostructures has estimated to

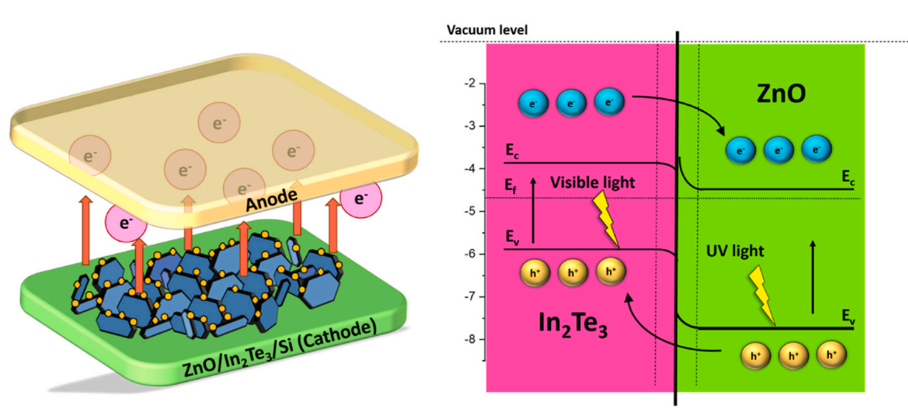


**Fig. 4.** Schematic Diagram of Fowler-Nordheim (F–N) of $In_2Te_3$/ZnO nanoheterostructures.

come about 3623. Therefore, it would be expected that $In_2Te_3$/ZnO based nanoheterostructures have enormous applications in field emission display devices, super capacitors, and solar cells.

## Notes

The authors declare no completing financial interest.

## CRediT authorship contribution statement

**Muhammad Safdar:** Conceptualization, Methodology, Software, Supervision, Writing – review & editing. **Muhammad Waqas:** Data curation, Writing – original draft, preparation, Methodology, Software. **Nimra Jabeen:** Visualization, Investigation. **Ahmad Saeed:** Visualization, Investigation. **Faheem K. Butt:** Software, Validation. **Shahzad Murtaza:** Reviewing. **Misbah Mirza:** Reviewing and Editing.

## Declaration of competing interest

The authors declare the following financial interests/personal relationships which may be considered as potential competing interests:

Muhammad Safdar reports financial support was provided by Higher Education Commission Pakistan.

## Data availability

No data was used for the research described in the article.

## Acknowledgment

This work was supported by the HEC, Pakistan funded Program NRPU (NRPU/R&D/HEC/2020–11749).

## Appendix A. Supplementary data

Supplementary data to this article can be found online at https://doi.org/10.1016/j.matchemphys.2022.126510.

## References

[1] A. Di Bartolomeo, A. Grillo, F. Giubileo, L. Camilli, J.B. Sun, D. Capista, M. Passacantando, Field emission from two-dimensional GeAs, J. Phys. Appl. Phys. 54 (2021).
[2] Y.L. Chu, S.J. Young, L.W. Ji, T.T. Chu, C.H. Wu, UV-enhanced field-emission performances of Pd-adsorbed ZnO nanorods through photochemical synthesis, ECS J. Solid-State Sci. Technol. 10 (2021).
[3] B.J. Yang, J.T. Chen, X.N. Wu, B. Liu, L.Y. Liu, Y. Tang, X.B. Yan, Enhanced field emission performance of MXene-TiO2 composite films, Nanoscale 13 (2021) 7622–7629.
[4] A.B. Deore, M.A. More, B.B. Musmade, S.D. Nerkar, P.G. Chavan, P.M. Koinkar, Photo-enhanced field-emission behavior of CdSSe microflowers, Int. J. Mod. Phys. B 35 (2021).
[5] Z. Ali, M. Mirza, C.B. Cao, F.K. Butt, M. Tanveer, M. Tahir, I. Aslam, F. Idrees, M. Safdar, Wide range photodetector based on catalyst free grown indium selenide microwires, ACS Appl. Mater. Interfaces 6 (2014) 9550–9556.
[6] M. Safdar, Q.S. Wang, Z.M. Wang, X.Y. Zhan, K. Xu, F.M. Wang, M. Mirza, J. He, Weak antilocalization effect of topological crystalline insulator Pb1-xSnxTe nanowires with tunable composition and distinct {100} facets, Nano Lett. 15 (2015) 2485–2490.
[7] A. Datta, D. Mukherjee, M. Hordagoda, S. Witanachchi, P. Mukherjee, R.V. Kashid, M.A. More, D.S. Joag, P.G. Chavan, Controlled Ti seed layer assisted growth and field emission properties of Pb (Zr0. 52Ti0. 48) O3 nanowire arrays, ACS Appl. Mater. Interfaces 5 (2013) 6261–6267.
[8] S. Xie, J. Huang, Y. Zhang, W. Cai, X. Zhang, Effect of substrate types on the structure of vertical graphene prepared by plasma-enhanced chemical vapor deposition, Nanomaterials 11 (2021) 1268.
[9] Z.L. Wang, Z.W. Pan, Junctions and networks of SnO nanoribbons, Adv. Mater. 14 (2002) 1029–1032.
[10] C. Tan, H. Zhang, Wet-chemical synthesis and applications of non-layer structured two-dimensional nanomaterials, Nat. Commun. 6 (2015) 1–13.
[11] D. Li, M.B. Müller, S. Gilje, R.B. Kaner, G.G. Wallace, Nat. Nanotechnol. 3 (2008) 101–105.
[12] P. Chaware, A. Nande, S. Dhoble, K. Rewatkar, Structural, photoluminescence and Judd-Ofelt analysis of red-emitting Eu3+ doped strontium hexa-aluminate nanophosphors for lighting application, Opt. Mater. 121 (2021), 111542.
[13] V.S. Bagal, G.P. Patil, A.B. Deore, P.K. Baviskar, S.R. Suryawanshi, M.A. More, P. G. Chavan, High current density and low turn-on field from aligned Cd (OH) 2 nanosheets, Chem. Phys. Lett. 650 (2016) 7–10.
[14] V. Gurylev, T.-K. Chin, A. Useinov, Charge transfer and field emission characteristics of TiO2@ CNTs nanocomposite: effect of TiO2 crystallinity, J. Alloys Compd. 857 (2021), 157598.
[15] S.-H. Kwon, T.-H. Kim, S.-M. Kim, S. Oh, K.-K. Kim, Ultraviolet light-emitting diode-assisted highly sensitive room temperature NO 2 gas sensors based on low-temperature solution-processed ZnO/TiO 2 nanorods decorated with plasmonic Au nanoparticles, Nanoscale 13 (2021) 12177–12184.
[16] S. Ahmed, J. Qiao, P.K. Cheng, A.M. Saleque, M.N.A.S. Ivan, T.I. Alam, Y.H. Tsang, Two-dimensional gallium sulfide as a novel saturable absorber for broadband ultrafast photonics applications, ACS Appl. Mater. Interfaces 13 (2021) 61518–61527.
[17] S.-J. Young, Y.-L. Chu, Characteristics of field emitters on the basis of Pd-adsorbed ZnO nanostructures by photochemical method, ACS Appl. Nano Mater. 4 (2021) 2515–2521.
[18] T. Zhai, L. Li, Y. Ma, M. Liao, X. Wang, X. Fang, J. Yao, Y. Bando, D. Golberg, One-dimensional inorganic nanostructures: synthesis, field-emission and photodetection, Chem. Soc. Rev. 40 (2011) 2986–3004.
[19] Y. Cao, H.A. Dhahad, M. El-Shorbagy, H.Q. Alijani, M. Zakeri, A. Heydari, E. Bahonar, M. Slouf, M. Khatami, M. Naderifar, Green synthesis of bimetallic ZnO–CuO nanoparticles and their cytotoxicity properties, Sci. Rep. 11 (2021) 1–8.
[20] M.-T. Tran, N.D. Hung, Q.N. Van, N.T. Huyen, N. Tu, H.P. Thanh, Emission-tunable Mn-doped ZnS/ZnO heterostructure nanobelts for UV-pump WLEDs, Opt. Mater. 121 (2021), 111587.
[21] T.R. Gurugubelli, R. Ravikumar, R. Koutavarapu, Structural, optical, and luminescence properties of Ni2+-doped ZnO–CdS nanocomposite: synthesis and investigations for green light emission, Chem. Pap. 76 (2022) 557–566.
[22] E.O. Ichipi, S.M. Tichapondwa, E.M. Chirwa, Plasmonic effect and bandgap tailoring of Ag/Ag2S doped on ZnO nanocomposites for enhanced visible-light photocatalysis, Adv. Powder Technol. 33 (2022), 103596.
[23] C. Krataithong, K. Srichai, E. Wongrat, A. Tubtimtae, Comparative study on the influence of transparent glass substrates for antimony telluride thin films via structural and optical properties, J. Sci.: Adv. Mater. Dev. 7 (2022), 100449.
[24] T. Jing, D. Liang, X. Huang, M. Deng, S. Cai, W. Liu, Controllable Schottky barriers by ferroelectric switching in graphene/In2Te3 heterostructures, J. Phys. Appl. Phys. 55 (2021), 015105.
[25] J. Zhen, W. Deng, C. Li, J. Feng, S. Zhang, S. Wan, G. Wang, H. Dong, R.A. Susilo, B. Chen, Superconductivity in In2Te3 under compression induced by electronic and structural phase transitions, J. Phys. Chem. Lett. 13 (2022) 1226–1233.
[26] M. Safdar, X. Zhan, M. Niu, M. Mirza, Q. Zhao, Z. Wang, J. Zhang, L. Sun, J. He, Site-specific nucleation and controlled growth of a vertical tellurium nanowire array for high performance field emitters, Nanotechnology 24 (2013), 185705.
[27] C. Song, K. Yu, H. Yin, H. Fu, Z. Zhang, N. Zhang, Z. Zhu, Highly efficient field emission properties of a novel layered VS 2/ZnO nanocomposite and flexible VS 2 nanosheet, J. Mater. Chem. C 2 (2014) 4196–4202.
[28] J. Yao, Z. Deng, Z. Zheng, G. Yang, Stable, fast UV–Vis–NIR photodetector with excellent responsivity, detectivity, and sensitivity based on α-In2Te3 films with a direct bandgap, ACS Appl. Mater. Interfaces 8 (2016) 20872–20879.
[29] M. Safdar, Z. Wang, M. Mirza, C. Jiang, J. He, Crystalline indium sesquitelluride nanostructures: synthesis, growth mechanism and properties, J. Mater. Chem. 22 (2012) 19228–19235.
[30] H. Lu, K. Deng, Z. Shi, Q. Liu, G. Zhu, H. Fan, L. Li, Novel ZnO microflowers on nanorod arrays: local dissolution-driven growth and enhanced light harvesting in dye-sensitized solar cells, Nanoscale Res. Lett. 9 (2014) 1–8.
[31] Y.-H. Tan, K. Yu, J.-Z. Li, H. Fu, Z.-Q. Zhu, MoS2@ ZnO nano-heterojunctions with enhanced photocatalysis and field emission properties, J. Appl. Phys. 116 (2014), 064305.
[32] G. Nabi, C. Cao, W.S. Khan, S. Hussain, Z. Usman, M. Safdar, S.H. Shah, N.A. D. Khattak, Synthesis, characterization, growth mechanism, photoluminescence and field emission properties of novel dandelion-like gallium nitride, Appl. Surf. Sci. 257 (2011) 10289–10293.
[33] S.-J. Young, Y.-H. Liu, J.-T. Chien, Improving field electron emission properties of ZnO nanosheets with Ag nanoparticles adsorbed by photochemical method, ACS Omega 3 (2018) 8135–8140.
[34] C. Gu, H. Huang, J. Huang, Z. Jin, H. Zheng, N. Liu, M. Li, J. Liu, F. Meng, Chlorobenzene sensor based on Pt-decorated porous single-crystalline ZnO nanosheets, Sensor Actuator Phys. 252 (2016) 96–103.